A dynamical mean-field theory study of Nagaoka ferromagnetism.

Hyowon Park, K. Haule, C. A. Marianetti, and G. Kotliar
Department of Physics and Astronomy and Center for Condensed
Matter Theory, Rutgers University, Piscataway, NJ 08854–8019
(Dated: August 31, 2007)

We revisit Nagaoka ferromagnetism in the two-dimensional $U = \infty$ Hubbard model using the dynamical mean-field theory (DMFT). A recently developed continuous time quantum Monte Carlo method is applied to solve the DMFT impurity problem. The stability of Nagaoka ferromagnetism is studied as a function of both the nearest-neighbor lattice hopping t and the next-nearest-neighbor lattice hopping t'. It is shown that the ferromagnetic state is strongly stabilized when t' is negative. A second order ferromagnetic to paramagnetic transition at $t' = 0$ changes to a first order transition at $t'/t = -0.1$. At a finite temperature T close to half filling, ferromagnetism becomes unstable as T exceeds the coherence temperature T_{coh}, while in the large doping regime the ferromagnetism emerges from a more conventional fermi liquid . We use the DMFT results to benchmark slave-boson calculations which can be used to study more complicated geometries.

I. INTRODUCTION

The possibility of the existence of a ferromagnetic phase in the $U = \infty$ Hubbard model is a long standing question. Nagaoka[1] showed that for a single hole in a bipartite lattice the ground state is a fully polarized ferromagnet, and the term "Nagaoka ferromagnetism" is commonly used to describe this state. Whether a fully or a partially polarized phase persist for a finite hole density (δ) has been a subject of numerous investigations[2].

The problem has been addressed with variational wave functions [3–7], slave particle methods [8,9], quantum Monte Carlo (QMC) methods[10], and variational QMC methods[11]. In all these methods the ferromagnetism survives up to a critical value of doping δ_c. It is known from these approaches that the size of the ferromagnetic region depends strongly on the lattice through the electronic dispersion. Even for one hole in the $U = \infty$ square lattice with a small positive next-nearest neighbor hopping t', the ferromagnetic state is unstable[12]. At an intermediate or a large U, a flat band below the Fermi level [13] or a peak in the density of states below the Fermi level [14–16], as realized in the fcc lattice[17,18] or a Van Hove singularity[19], stabilize the ferromagnetic state.

The dynamical mean-field theory (DMFT) has also been used to address the Nagaoka problem, however the number of impurity solvers available to reach the $U = \infty$ limit is very limited. Obermeier *et al.*[20] carried out the first DMFT study of this problem using the non-crossing approximation as an impurity solver, and they confirmed a ferromagnetic state below a critical temperature T_c in the hypercubic lattice in infinite dimensions. The existence of a ferromagnetic state in this model was confirmed using the numerical renormalization group as an impurity solver[21].

In this study, we revisit the problem of Nagaoka ferromagnetism in the $U = \infty$ Hubbard model within DMFT, using the recently developed continuous time quantum Monte Carlo (CTQMC) as an impurity solver[22,23]. This impurity solver allows the numerically exact solution of the DMFT equations for all values of δ and at very low

temperatures for $U = \infty$. We find that at large doping, the ferromagnetism emerges from a conventional Fermi liquid, while at small doping the Curie temperature is very close to the coherence temperature, hence the ferromagnetism emerges from an incoherent state. We pay particular attention to the possibility of phase separation and its dependence on the sign of t'/t. Finally we benchmark simpler approaches to the problem such as the slave boson method, and we identify the physical quantities for which this method, in spite of its simplicity and limitations, is remarkably accurate. This is important since the detailed modeling of optical lattices of cold atoms, which provide a clean realization of the Hubbard model, will require incorporating spatial inhomogeneities into the treatments of strong correlations. At present, this can only be done with simpler techniques such as slave bosons methods.

We study the Hamiltonian of the $U = \infty$ Hubbard model given by.

$$\hat{H} = -\sum_{ij\sigma} t_{ij} \hat{P}_s \hat{c}_{i\sigma}^\dagger \hat{c}_{j\sigma} \hat{P}_s \tag{1}$$

where $\hat{P}_s$ is a projection operator which removes states with double-occupied sites. We consider both nearest-neighbor (n.n) hopping t and next-nearest-neighbor (n.n.n) hopping t'. The units are fixed by choosing $t = \frac{1}{2}$.

II. A DMFT+CTQMC APPROACH

DMFT maps the partition function of the Hubbard model onto the partition function of an effective Anderson impurity model (AIM) resulting in the following effective action.

$$S_{eff} = S_{atom} + \int_0^\beta d\tau \int_0^\beta d\tau' \sum_\sigma c_\sigma^\dagger(\tau) \Delta_\sigma(\tau - \tau') c_\sigma(\tau') \tag{2}$$

where S_{atom} represents the action of the isolated impurity, and $\Delta_\sigma(\tau - \tau')$ is the hybridization function of the

effective AIM. In this $U = \infty$ case, the double occupied state of the impurity should be excluded when evaluating S_{atom}. $\Delta_\sigma(\tau - \tau')$ is not initially known and it must be determined by the DMFT self-consistency condition given below. The impurity Green function and the impurity self-energy are given by the following equations

$$G_\sigma(\tau - \tau') = -\langle T c_\sigma(\tau) c_\sigma^\dagger(\tau') \rangle_{S_{eff}} \quad (3)$$

$$\Sigma_\sigma(i\omega_n) = i\omega_n + \mu - \Delta_\sigma(i\omega_n) - G_\sigma^{-1}(i\omega_n). \quad (4)$$

The DMFT self-consistency condition requires that the self-energy of the lattice is equivalent to the self-energy of the effective AIM, and that the local Green's function of the lattice is equivalent to the Green's function of the effective AIM

$$\sum_{\mathbf{k}} \frac{1}{i\omega_n + \mu + h\sigma - \epsilon(\mathbf{k}) - \Sigma_\sigma(i\omega_n)}$$
$$= \frac{1}{i\omega_n + \mu + h\sigma - \Delta_\sigma(i\omega_n) - \Sigma_\sigma(i\omega_n)}, \quad (5)$$

where $\epsilon(\mathbf{k}) = -2t(\cos k_x + \cos k_y) - 4t' \cos k_x \cos k_y$ and h is the external magnetic field. For a given hybridization $\Delta_\sigma(i\omega_n)$, the effective action S_{eff} is constructed and the AIM is solved for the new $G_\sigma(i\omega_n)$ and $\Sigma_\sigma(i\omega_n)$. This iterative procedure continues until the Green function is converged.

To solve the impurity problem (Eq. 2), CTQMC is used as the impurity solver. In CTQMC, the hybridization part of the effective action is treated as a perturbation around the atomic part and all diagrams are summed up by stochastic Metropolis sampling.[23] In this $U = \infty$ case, doubly occupied state of the atom is excluded from atomic eigenstates. CTQMC converges well in the low Matsubara frequency region, but it is poorly behaved in the high frequency region. Therefore, one needs the analytic expression for the self-energy in the high frequency limit and it has to be interpolated to the low frequency region. The lowest order $\Sigma_\sigma(\infty)$ in the $U = \infty$ Hubbard model is related to the high frequency moments of Green's function as follows:

$$Re[\Sigma_\sigma(\infty)] = m_{1\sigma}/m_{0\sigma}^2 + \mu \quad (6)$$

$$Im[\Sigma_\sigma(\infty)] = (1 - 1/m_{0\sigma})\omega \quad (7)$$

where $m_{0\sigma} = \langle \{c_\sigma, c_\sigma^\dagger\} \rangle = 1 - n_{-\sigma}$, $m_{1\sigma} = \langle \{[c_\sigma, H], c_\sigma^\dagger\} \rangle = -\mu(1 - n_{-\sigma}) - Tr[\Delta_{-\sigma} G_{-\sigma}]$.

CTQMC can calculate various spin dependent physical quantities such as occupation numbers $(n_\uparrow, n_\downarrow)$ and the local magnetic susceptibility (χ_{loc}). The $q = 0$ magnetic susceptibility of a lattice can be calculated from χ_{loc} by evaluating complicated vertex functions. To circumvent this difficulty, $\chi_{q=0}$ of a lattice can be calculated from the ratio of magnetization to the external magnetic field $(\chi = \frac{dm}{dh}|_{h=0})$. The external field h alters the effective action (Eq. 2) by adding $h\sigma$ to atomic energies and the self-consistency condition (Eq. 5) is enforced to include the

spin dependent $h\sigma$ term during DMFT iterations. The exclusion of the double occupancy $(U = \infty)$ implies the Hubbard potential energy to vanish and the only relevant energy is the kinetic energy. The kinetic energy of spin σ electrons in a AIM is given by $Tr[\Delta_\sigma G_\sigma]$, and it is related to the average of the perturbation order k as follows:

$$E_{kin,\sigma} = Tr[\Delta_\sigma G_\sigma] = -T\langle k_\sigma \rangle \quad (8)$$

where T is temperature. Therefore, it is possible to calculate the kinetic energy precisely by evaluating $\langle k_\sigma \rangle$. The free energy, F, can also be derived from the kinetic energy as long as it is in the fermi liquid regime.

$$F(T) \cong E_{kin} - \frac{\pi^2}{3} Z^{-1} \rho_0(\mu) T^2 \quad (9)$$

where Z is the renormalization residue and ρ_0 is the non-interacting density of states.
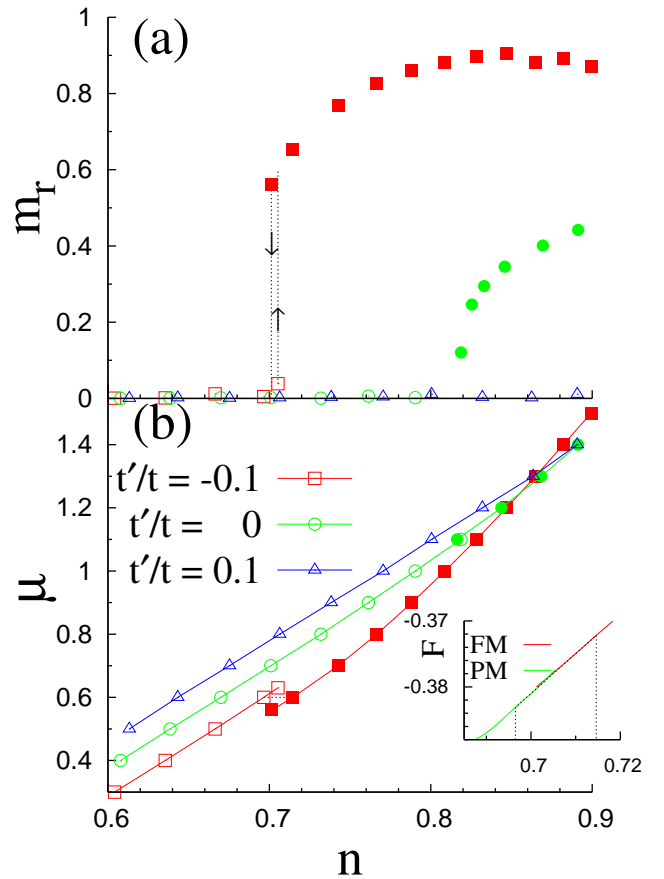

FIG. 1: (Color online) (a) The reduced magnetization $m_r=(n_\uparrow - n_\downarrow)/(n_\uparrow + n_\downarrow)$ vs the electron density n at t'/t=-0.1, 0, and 0.1 (b) the chemical potential μ vs n at t'/t=-0.1, 0, and 0.1. Filled points indicate a FM state. Inset : FM free energy and PM free energy vs n at t'/t=-0.1. The dotted line is constructed using the Maxwell construction. All calculations were performed at T=0.01.
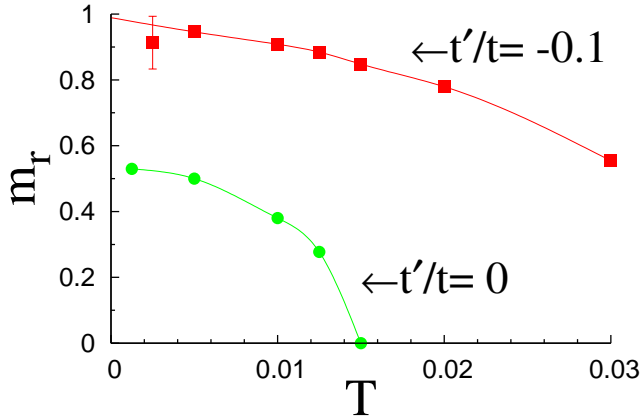
FIG. 2: (Color online) m_r vs T at fixed n =0.85 with t'/t=-0.1 and 0. The fully polarized FM state ($m_r = 1$) is expected only when t'/t=-0.1.

Fig. 1.(a) shows the reduced magnetization m_r=$(n_\uparrow - n_\downarrow)/(n_\uparrow + n_\downarrow)$ as a function of the electron density n at three distinct t'/t ratios. The result is notably different as t'/t varies, with the spontaneously broken ferromagnetic (FM) state ($m_r \neq 0$) being favored for $t'/t < 0$ and eventually becoming unstable for $t'/t > 0$. The critical density (n_c) at which the transition occurs increases as t'/t increases to a positive value, reducing the FM region. Moreover, at $t'/t = -0.1$ m_r changes abruptly at n_c=0.705 indicating a first order transition, while at $t'/t = 0$ m_r increases continuously indicating a second order transition at n_c=0.815.

Notice that close to half filling the Curie temperature becomes small and at fixed temperature ($T = 0.01$) it becomes increasingly difficult to converge the DMFT equations near the transition temperature due to the standard critical slowing down.

Near half filling the quasiparticle bandwidth becomes small due to the strong correlations hence the thermal fluctuations become comparable to the Curie temperature in this region.

A stable FM state is possible again if T is lowered sufficiently below T_{coh}. In the region above 0.95, an incoherent paramagnetic (PM) state becomes stable as T exceeds T_{coh}. Inspecting the chemical potential as a function of density reveals that the nature of the transition changes with t'/t (see figure 1.(b)). For $t'/t = -0.1$, there is a region of constant chemical potential which corresponds to a first-order transition, while for $t'/t = 0$ the transition is continuous. The flat chemical potential region ($n = 0.696 - 0.715$) indicates that two different DMFT solutions (FM, PM) can be converged depending on the initial conditions and it indicates phase separation (PS) of the FM and PM state. This region is determined by Maxwell construction which connects common tangents between two phases in the free energy vs n graph. (Fig. 1. inset)
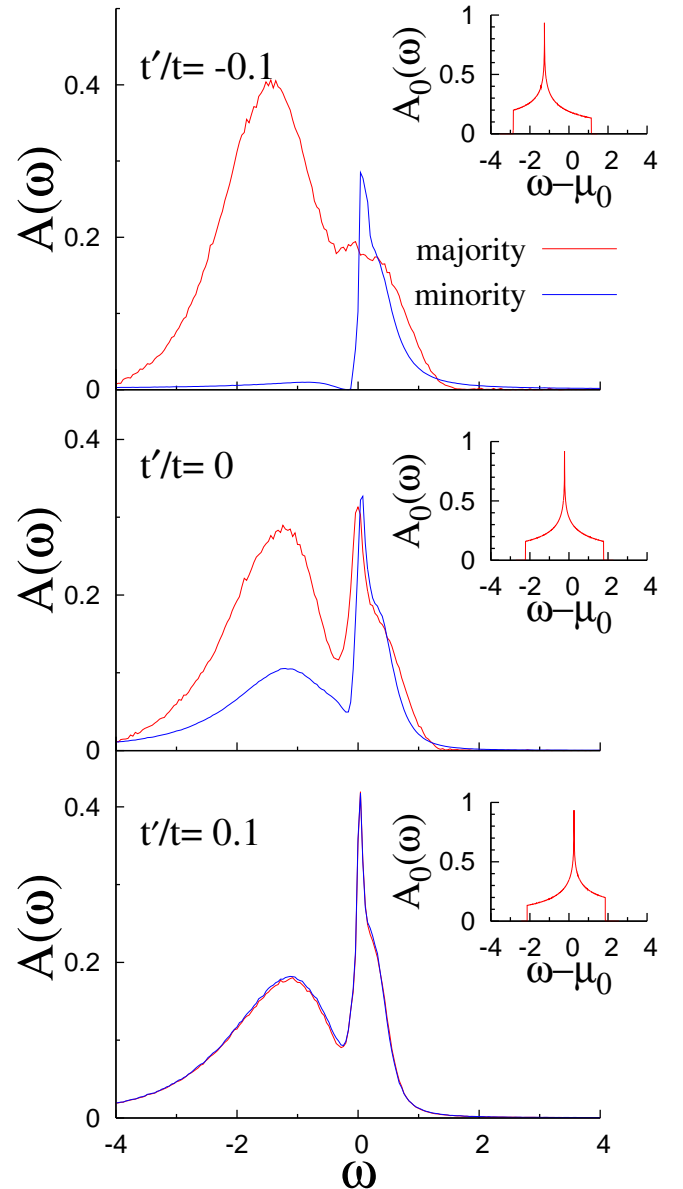

FIG. 3: (Color online) The spectral functions $A(\omega)$ at t'/t=-0.1 (top), 0 (middle), and 0.1 (bottom) for fixed n =0.85. Inset: Non-interacting spectral functions ($A_0(\omega)$) of the majority spin at the corresponding t'/t values. ($\mu_0 = \mu - Re\Sigma(0)$) All calculations were performed at T=0.01.

The original debate on the Nagaoka problem was focused on the existence of the fully polarized FM state at finite δ in the $T \to 0$ limit. Therefore, it is necessary to investigate m_r at very low T. Fig. 2 shows that the fully polarized Nagaoka state is not stabilized at least when $\delta = 0.15$ and $t'/t = 0$. Nevertheless, at $t'/t = -0.1$, the fully polarized FM state is realized. As the spins become fully polarized ($t'/t = -0.1, T \to 0$), numeric requires high statistics and an error-bar is specified to take into
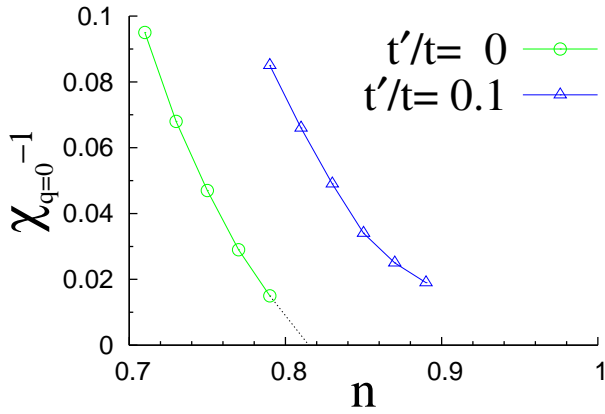
FIG. 4: (Color online) The uniform susceptibility ($\chi_{q=0}^{-1}$) vs n at $t'/t = 0$ and 0.1. The dotted line is for the extrapolation to $\chi_{q=0}^{-1} = 0$. (T=0.01)
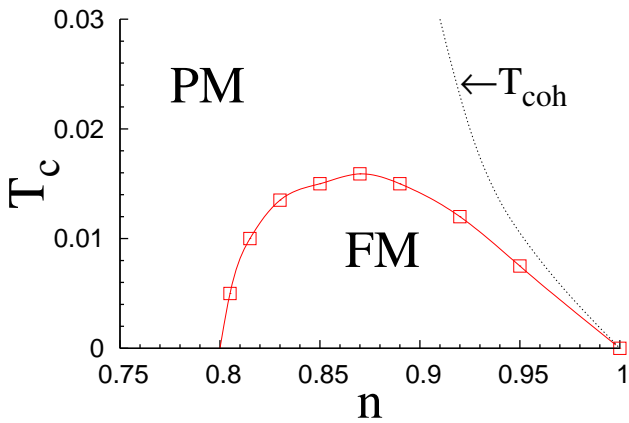

FIG. 5: (Color online) The critical temperature T_c vs n at $t' = 0$. n_c at $T = 0$ is obtained from the extrapolation. The dotted line represents the coherence temperature T_{coh} vs n.

FIG. 6: (Color online) The local susceptibility (χ_{loc}^{-1}) vs T and the uniform susceptibility ($\chi_{q=0}^{-1}$) vs T ($t'/t = 0$)

account the numerical error.

The spectral functions on the real frequency axis are shown in Fig. 3. Because CTQMC works on the imaginary frequency axis, one needs to perform the analytical continuation of the Green function to the real axis. Here we use the maximum entropy method[24]. The spectral functions show noticeable differences to small perturbations in t' at fixed n=0.85. At $t'/t = -0.1$, the majority spin spectral function shows no quasiparticle peak and large spectral weight at $\omega < 0$. The overall shape is similar to the non-interacting spectral function (Fig. 3. inset). The minority spin spectral function has a narrow quasiparticle band and a small lower Hubbard band. The quasiparticle band narrows by a factor Z. At $t'/t = 0$ and $t'/t = 0.1$, the spectral functions consist of a narrow quasiparticle band and a lower Hubbard band, similar to the minority spin state for $t'/t = -0.1$. In the $U = \infty$
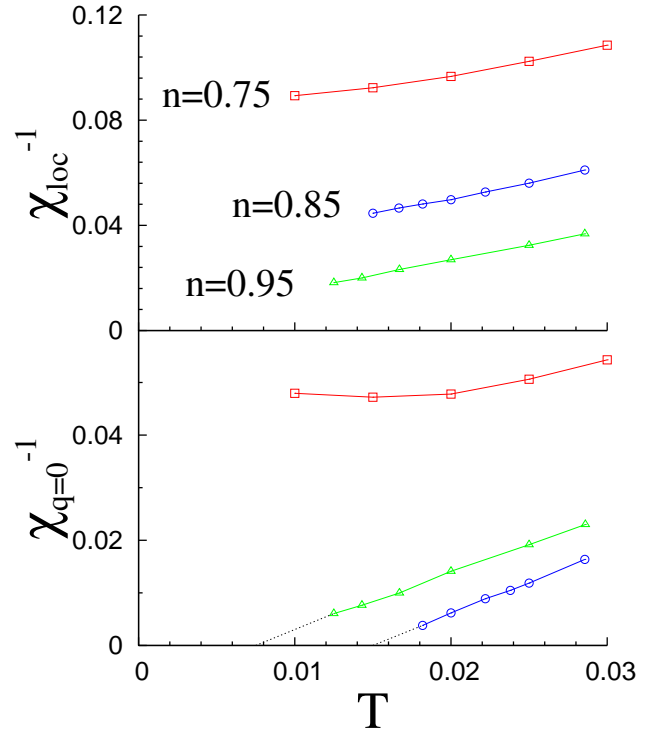
Hubbard model, the upper Hubbard band disappears due to the exclusion of double occupancy. The stability of the FM state at $t'/t = -0.1$ originates from the large spectral weight of the $\omega < 0$ region making the FM state energetically stable. This is a consequence of the non-interacting DOS shown in the inset of Fig. 3.

The inverse of the $q = 0$ magnetic susceptibility ($\chi_{q=0}^{-1}$) of the PM state vs n at $t'/t = 0$ and 0.1 is shown in Fig. 4. The extrapolated line at $t' = 0$ indicates that χ diverges near $n = 0.815$, confirming the second order transition at the critical density ($n_c = 0.815$). At $t'/t = 0.1$, one might expect χ will diverge near $n = 1$. However, as T_{coh} becomes smaller than T near $n = 1$, the incoherent PM state is stabilized. In other words, at $t'/t = 0.1$, the crossover from the coherent PM state to the incoherent PM state occurs instead of the transition to the FM state.

Fig. 5 shows the critical temperature (T_c) vs n at $t'/t = 0$. In the region below T_c a partially polarized FM state is found, and it is determined by observing $n_\uparrow \neq n_\downarrow$ in a CTQMC result. This graph shows that the lower critical density (n_c) at $T = 0$ is about 0.8. At half filling critical temperature should vanish due to the following reason. The kinetic energy at half filling is zero in both the paramagntic and ferromagnetic state because of the blocking of charge density. The entropy of the paramagnet is much larger than the entropy of the ferromagnet due to the large spin degeneracy of the paramagnetic state. In other words, PM state is thermodynamically
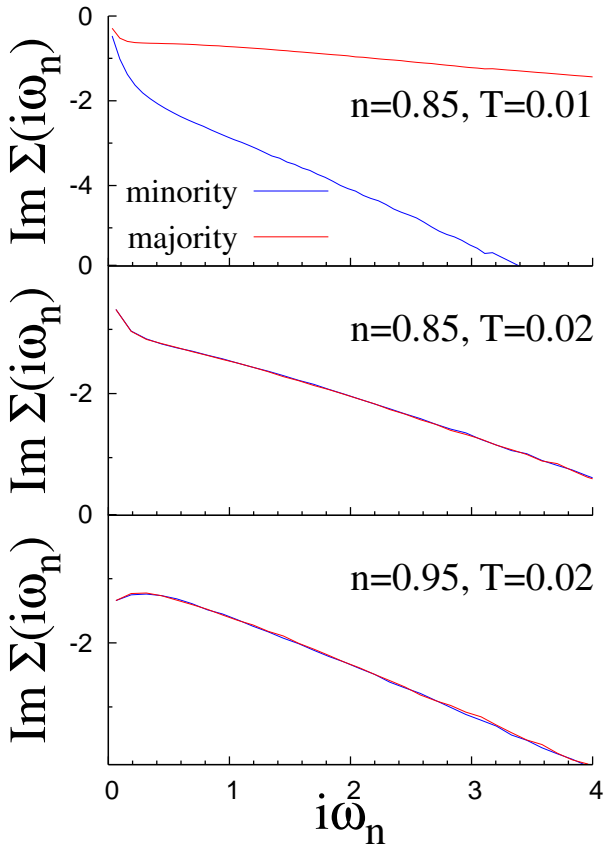
FIG. 7: (Color online) $Im\Sigma(i\omega_n)$ vs $i\omega_n$ at the coherent FM state (the top panel), the coherent PM state (the middle panel), and the incoherent PM state (the bottom panel). ($t'/t = 0$)

(Fig. 6). $\chi_{q=0}^{-1}$ near a transition point obeys the Curie-Weiss form ($\chi_{q=0}^{-1} \sim T - T_c$). Both coherent ($n = 0.85$) and incoherent ($n = 0.95$) regions show linear dependence of $\chi_{q=0}^{-1}$ on T. The $\chi_{q=0}^{-1}$ for $n = 0.75$ barely depends on T, exhibiting Pauli paramagnetic behavior. χ_{loc}^{-1} is greater than $\chi_{q=0}^{-1}$ and it increases as n decreases. This is because in DMFT $\chi_{loc}^{-1} \sim T + T_{coh}$ and T_{coh} increases as n decreases[25].

Fig. 7 shows the behavior of $Im\Sigma(i\omega_n)$ for the three different phases in the T_c phase diagram of Fig. 5. For $n = 0.85$ and $T = 0.01$, a coherent FM state is expected from the phase diagram. A coherent Fermi liquid is validated by investigating the negative slope of $Im\Sigma(i\omega_n)$ at $\omega = 0$. The slope for spin σ at the high frequency part is given by $-n_{-\sigma}/1 - n_{-\sigma}$ (Eq. 7) and the inequality of the slope indicates $n_\uparrow \neq n_\downarrow$ confirming FM state. The majority spin state has a smaller slope at high frequency because $n_{-\sigma}$ of the majority spin is smaller than that of the minority spin. Also, because the slope of the majority spin at $\omega = 0$ is smaller, Z of the majority spin is larger than that of the minority spin. This means the quasiparticle band of the minority spin is more renormalized by strong correlations while the majority spin state tends to be similar to the non-interacting energy dispersion. For $n = 0.85$ and $T = 0.02$, a coherent PM state is established by observing a negative slope at $\omega = 0$ and no spin symmetry breaking. For $n = 0.95$ and $T = 0.02$, an incoherent PM state is expected from the positive slope at $\omega = 0$ because the concept of Z is no longer valid and the application of Fermi liquid theory fails. Lastly, for fixed $T = 0.02$, as n increases from 0.85 to 0.95 the slope at high frequency also increases because $n_{-\sigma}$ increases.

stable at any finite temperature at $n = 1$.

As the width of the quasiparticle band becomes smaller near $n = 1$, T_{coh} is also reduced making it hard to sustain the quasiparticle peak. At $T > T_{coh}$, the PM state is clearly stabilized. The T_{coh} boundary can be determined from the imaginary part of self energy ($Im\Sigma(i\omega_n)$) on the imaginary frequency axis. In a coherent region ($T < T_{coh}$), the renormalization residue Z is well defined ($0 < Z < 1$) by evaluating the negative slope of $Im\Sigma(i\omega_n)$ at $\omega = 0$. ($Z = (1 - \frac{dIm\Sigma}{d\omega}|_{\omega=0})^{-1}$). However, in the incoherent regime ($T > T_{coh}$), the slope of $Im\Sigma(i\omega_n)$ at $\omega = 0$ becomes positive making the concept of Z ill defined (Fig. 7). Therefore, we determined T_{coh} as the temperature where the slope of the low energy self energy vanishes, and found that it is almost proportional to $\delta^{3/2}$, in surprising agreement with the findings of a previous study of doped Mott-insulator[25].

In general, $n_\uparrow - n_\downarrow$ exhibits small fluctuations near the boundary of T_c due to the finite T. The fluctuations become especially severe through the transition from the FM state to the incoherent PM state near $n = 1$. Therefore, the boundary points can be determined more precisely by examining the temperature dependence of $\chi_{q=0}^{-1}$

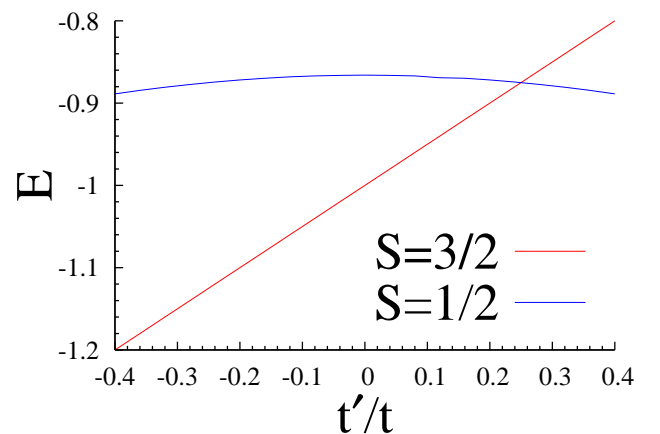## III. NAGAOKA FERROMAGNETISM FROM A 4-SITE PLAQUETTE

FIG. 8: (Color online) The lowest energies of a S=1/2 state and a S=3/2 state in a $U = \infty$ 4-site toy model varying t'/t. E is the energy in units of $t = 1/2$.

In order to provide a simple interpretation of why decreasing t' stabilizes the Nagaoka state, we examine the simplest possible model which retains the physics of the Nagaoka problem. We consider a 4-site plaquette with three electrons (one hole). The ground state of this model may be characterized by the quantum number corresponding to the total spin angular momentum (ie. $S = \frac{3}{2}, \frac{1}{2}$) and the z-direction of the spin angular momentum ($S_z = \pm\frac{3}{2}, S_z = \pm\frac{1}{2}$). The whole Hamiltonian matrix is a 32×32 matrix excluding double-occupied sites and it is block-diagonalized to 6 distinct spin sectors by performing the unitary transform in the proper S, S_z basis. The ground state energy at each spin sector is determined by the exact diagonalization of Hamiltonian matrix.

The lowest energy in a $S = \frac{3}{2}$ sector is given by $-2t+t'$ and in the $S = \frac{1}{2}$ sector is given by $-\sqrt{3t^2 + t'^2}$. The energy dependence of a $S = \frac{3}{2}$ state is noticeably different from that of a $S = \frac{1}{2}$. In a $S = \frac{3}{2}$ case, doubly occupied states are excluded by the Pauli principle regardless of U. Therefore, the $U = \infty$ Hamiltonian is equivalent to the $U = 0$ Hamiltonian where the addition of the positive n.n.n hopping t' contributes linearly to the increase of the kinetic energy. However, doubly occupied states in a $S = \frac{1}{2}$ sector are excluded only for $U \to \infty$. Therefore, unlike the $S = \frac{3}{2}$ case, the energy dependence on t' is greatly reduced as the Hilbert space shrinks due to infinite U.

A $S = \frac{3}{2}$ ground state is indicative of the Nagaoka ferromagnetic state while a $S = \frac{1}{2}$ ground state is indicative of a paramagnetic state. The $S = \frac{3}{2}$ state is the ground state for $t'/t < 0.24$ and the energy difference increases approximately linearly thereafter indicating that the Nagaoka state is stabilized as t'/t is decreased. This is in agreement with the DMFT results presented in the previous section. The energy of the $S = \frac{1}{2}$ state weakly depends on t' while the $S = \frac{3}{2}$ energy decreases as t'/t decreases. This also explains that the stability of Nagaoka ferromagnetism originates from the minimization of the kinetic energy.

IV. A MEAN-FIELD SLAVE BOSON APPROACH

In this section, Nagaoka ferromagnetism in a two-dimensional $U = \infty$ Hubbard model will be studied using a mean-field slave boson approach. In a slave boson method, a fermion operator is accompanied by bosonic operators (ie. slave bosons) which keeps track of the local occupation number. The three slave boson operators are $\hat{e}, \hat{p}_\uparrow, \hat{p}_\downarrow$ and they act on unoccupied sites, spin-up sites, and spin-down sites, respectively. In this $U = \infty$ case, the doubly occupied sites are excluded. Constraints regarding the conservation of the occupation number are imposed with Lagrange multipliers ($\lambda, \lambda_\uparrow, \lambda_\downarrow$). The Hamiltonian is given in terms of the slave bosons as follows:

$$\hat{H} = -\sum_{ij\sigma} t_{ij}\hat{c}_{i\sigma}^\dagger \hat{z}_{i\sigma} \hat{z}_{j\sigma}^\dagger \hat{c}_{j\sigma} - \sum_{i\sigma} \lambda_{i\sigma}(\hat{p}_{i\sigma}^\dagger \hat{p}_{i\sigma} - \hat{c}_{i\sigma}^\dagger \hat{c}_{i\sigma}) +$$
$$\sum_{i\sigma} \lambda_i(\hat{p}_{i\sigma}^\dagger \hat{p}_{i\sigma} + \hat{e}_i^\dagger \hat{e}_i - 1) \qquad (10)$$

where $\hat{z}_{i\sigma} = \frac{1}{\sqrt{1-\hat{p}_{i\sigma}^\dagger \hat{p}_{i\sigma}}} \hat{e}_i^\dagger \hat{p}_{i\sigma} \frac{1}{\sqrt{1-\hat{e}_i^\dagger \hat{e}_i - \hat{p}_{i-\sigma}^\dagger \hat{p}_{i-\sigma}}}$. $t_{ij} = t$ if i,j are n.n, and $t_{ij} = t'$ if i,j are n.n.n. The non-interacting $\epsilon(\mathbf{k})$ is given by $-2t(\cos k_x + \cos k_y) - 4t' \cos k_x \cos k_y$ just as the DMFT case. The original Fock space has been enlarged including the slave boson fields. The partition function can be calculated from the Feynman functional path integral over the original fermi fields, slave boson fields, and Lagrange multipliers. The integral over the fermi fields is straightforward because the Hamiltonian is quadratic in the fermi fields. The integral over the slave boson fields and Lagrange multipliers should be performed using the saddle-point approximation, where the integral over the slave boson fields and Lagrange multipliers is approximated by putting their space and time independent mean-field values which minimize the Hamiltonian. The physical meaning of slave boson mean-field value is clear. The expectation value $\langle \hat{e}^\dagger \hat{e} \rangle$ corresponds to the fraction of unoccupied sites, i.e. the hole density $\delta(1 - n)$. Similarly, $\langle \hat{p}_\uparrow^\dagger \hat{p}_\uparrow \rangle$ equals to the spin up occupation number ($n_\uparrow$), and $\langle \hat{p}_\downarrow^\dagger \hat{p}_\downarrow \rangle$ corresponds to the spin down occupation number ($n_\downarrow$).

The free energy can be derived from the partition function ($F = -k_B T \ln Z$) and it is necessary to compare the free energies between ferromagnetic state and paramagnetic state to investigate the transition. The free energy is a function of magnetization $m = n_\uparrow - n_\downarrow$, δ, and T. At $T = 0$, the free energy becomes the ground state energy. The energies of the fully polarized ferromagnetic (FPFM) state ($m = n_\uparrow$) and the paramagnetic (PM) state ($m = 0$) are given by.

$$E_{FPFM}(\delta) = \frac{1}{N_s} \sum_\mathbf{k} \epsilon(\mathbf{k})\Theta(\mu - \epsilon(\mathbf{k})) \qquad (11)$$

$$E_{PM}(\delta) = \frac{1}{N_s} \sum_{\mathbf{k},\sigma} Z\epsilon(\mathbf{k})\Theta(\mu^* - Z\epsilon(\mathbf{k})) \qquad (12)$$

where N_s is the number of total sites, Z is the renormalization residue given by $2\delta/(1 + \delta)$, μ is the chemical potential in a fully polarized ferromagnetic state satisfying $(1/N_s) \sum_\mathbf{k} \Theta(\mu - \epsilon(\mathbf{k})) = n_\uparrow = 1 - \delta$, and $\mu^* = (\mu - \lambda_\sigma)$ is the effective chemical potential in a paramagnetic state satisfying $(1/N_s) \sum_\mathbf{k} \Theta(\mu^* - Z\epsilon(\mathbf{k})) = n_\uparrow = n_\downarrow = (1 - \delta)/2$. The DOS of the FPFM state is the same as the non-interacting DOS ($\rho_0(\epsilon)$) while the DOS of the PM state is renormalized by a factor Z to $1/Z \cdot \rho_0(\epsilon/Z)$. Unlike the DMFT method, the slave boson approach considers only the renormalized quasiparticle DOS ignoring the incoherent contribution. E_{PM} is given by $Z \cdot E_0$ where E_0 is the non-interacting energy. In other

words, as δ reduces to 0, the energy for a paramagnetic state is strongly renormalized by a factor $2\delta/(1+\delta)$ to avoid the doubly occupied states. That makes FM state more stable at small δ.
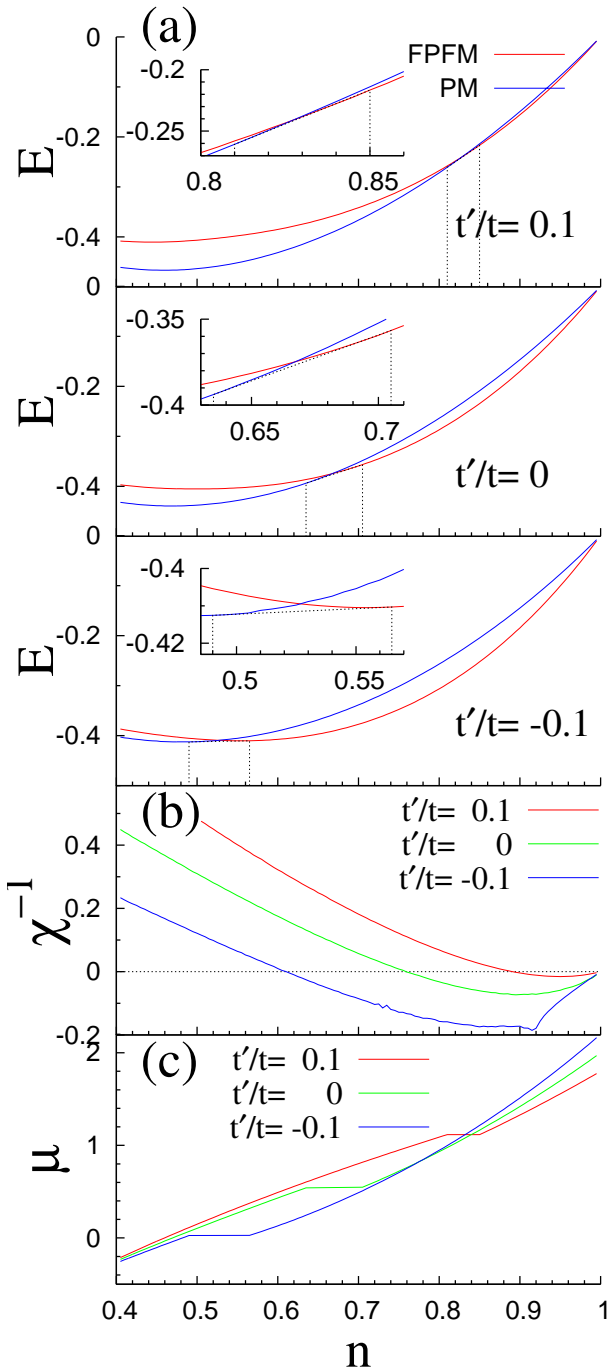

FIG. 9: (Color online) (a) The fully polarized ferromagnetic (FPFM) energy and paramagnetic (PM) energy vs n varying t'/t (0.1 (top), 0 (middle), and -0.1 (bottom)) Inset : Maxwell construction to determine the PS region. (b) The inverse of uniform magnetic susceptibility (χ^{-1}) at $m=0$ vs n varying t'/t (0.1, 0, and -0.1). (c) The chemical potential (μ) vs n at $t'/t = 0.1$, 0, and -0.1.

In Fig. 9.(a), fully polarized ferromagnetic (FPFM) energy and PM energy vs n are shown for $t'/t = 0.1, 0$, and -0.1. For all values of t'/t, the FPFM energy is stable at large n while the PM energy is stable at small n. The intermediate PS region is constructed by the Maxwell construction and is indicative of a fist order transition. At large n, as in the plaquette case, the energy curve for the paramagnet state depends weakly on t' while the FPFM energy curve becomes much lower as t'/t becomes negative. This results is in agreement with the previous DMFT results. As t'/t becomes more negative, the FPFM state is more stable and the critical density, n_c decreases. Just as in the DMFT, the large spectral weight of the non-interacting DOS at a low energy makes FPFM state energetically stable at $t'/t = -0.1$. When t' is 0, the energy difference between FPFM and PM is 0 at $n_c=2/3$ which agrees with the previous slave boson calculations[8,9].

We also calculate the inverse of uniform magnetic susceptibility (χ^{-1}) to study the instability of the PM state. The analytic expression is

$$\chi^{-1}|_{m=0} = \frac{1}{2\rho(\mu^*)} + \frac{2\mu^*}{1+\delta} +$$
$$\frac{1}{N_s}\sum_{\mathbf{k}} \frac{4}{(1+\delta)^2} Z\epsilon(\mathbf{k})\Theta(\mu^* - Z\epsilon(\mathbf{k})) \quad (13)$$

where $\rho(\mu^*)$ is the renormalized DOS given by $1/Z \cdot \rho_0(\mu^*/Z)$.

The trends in χ^{-1} are consistent with the results shown in Fig. 9.(a). As t'/t decreases, PM state becomes unstable ($\chi^{-1}=0$) at smaller n and it indicates FM state is mostly favored at $t'/t = -0.1$. (see Fig. 9 (b)) However, the instability of the PM state occurs at a larger density than n_c of Fig. 9 (a) which is indicative of a first order transition. At $t'/t = -0.1$, the high spectral peak at lower energy causes ρ to be larger at the fixed $n_\sigma(< 0.5)$ and it makes χ^{-1} smaller than other t'/ts. (Eq. 13)

Fig. 9 (c) shows the flat chemical potential region exists at any t'/ts in a μ vs n graph. This is the generic feature of first order transition and the region represents the coexistence of the FPFM and PM phase. This coexistence region is larger for negative t'/t favoring transition to the FM phase.

V. COMPARISON OF THE SLAVE BOSON RESULT AND THE DMFT+CTQMC RESULT

The slave boson method overestimates the region of the stable ferromagnetic state as compared to DMFT and it favors a first order transition (see Table 1). This is because the slave boson approach overestimates the paramagnetic kinetic energy as compared to the DMFT approach (Fig. 10). The quasiparticle residue Z of the DMFT approach is evaluated by $(1 - \frac{dIm\Sigma}{d\omega}|_{\omega=0})^{-1}$ on the imaginary frequency axis while Z of the slave boson approach is given by $2\delta/(1+\delta)$. Fig. 11 shows that

		$t'/t=-0.1$	$t'/t=0$	$t'/t=0.1$
DMFT	n_c	0.705	0.815	N/A
$(T=0.01)$	order	First	Second	N/A
Slave boson	n_c	0.53	0.67	0.83
$(T=0)$	order	First	First	First

TABLE I: n_c and the order of the ferromagnetism transition in a two-dimensional $U=\infty$ Hubbard model from both the DMFT+CTQMC approach and the slave boson approach with $t'/t=$ -0.1, 0, and 0.1. N/A means no transition to FM state occurs.
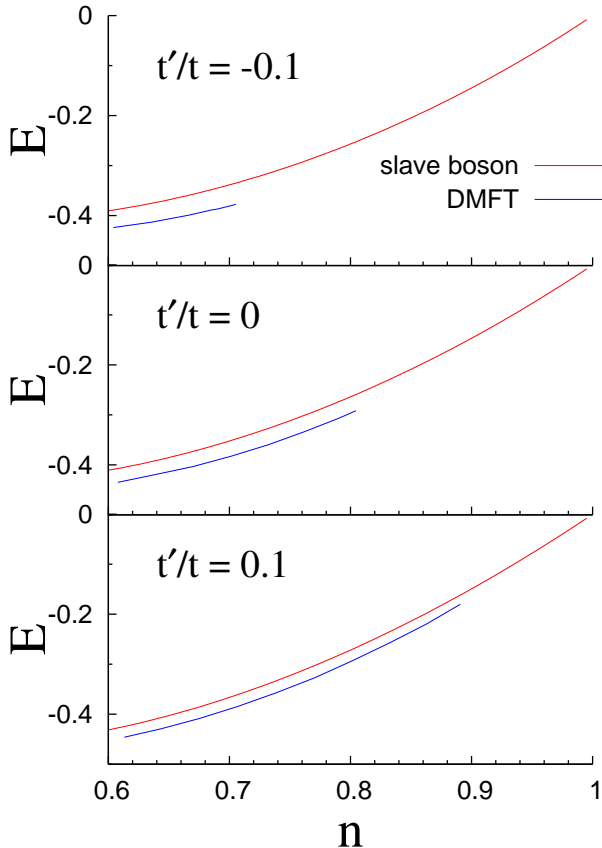

FIG. 10: (Color online) Paramagnetic energy from both the DMFT+CTQMC $(T=0.01)$ and the slave boson $(T=0)$ approach vs n at $t'/t=$-0.1 (the top panel), 0 (the middle panel), and 0.1 (the bottom panel).

Z of the slave boson study is overestimated as compared to the DMFT+CTQMC case. The slave boson technique used in this paper is based on the mean-field saddle-point approximation and it does not treat the strong correlation effect properly. Even though DMFT ignores the spatial correlation effect beyond a single site, the temporal correlations are treated exactly by CTQMC. Moreover, the mean-field slave boson approach evaluates the total energy as the sum of coherent quasiparticle energies (Eq. 12) while the total energy of DMFT+CTQMC includes contributions from both the incoherent and coherent effects. The over-estimated Z in the slave boson case
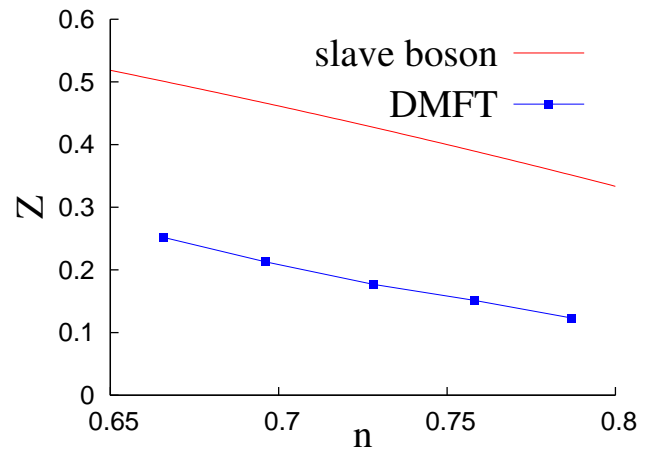

FIG. 11: (Color online) The renormalization residue (Z) of the slave boson method and the DMFT+CTQMC method ($t'=0$).

underestimates the kinetic energy while the ignorance of contribution from the incoherent part overestimates the energy. As a result, the two errors of the slave boson approach cancel each other giving a slightly overestimated energy as compared to the DMFT+CTQMC result.

Additionally, the χ^{-1} graph in the slave boson method almost coincides with the DMFT+CTQMC result comparing Fig. 4 and Fig. 9 (b). It is not certain how the renormalization residue Z affects χ^{-1} in the DMFT+CTQMC case, and the contribution from the incoherent part is also unclear. Therefore, further study will be required to fully understand the positive agreement of χ in the two methods.

VI. CONCLUSION

To summarize, we investigated Nagaoka ferromagnetism in a two-dimensional $U=\infty$ Hubbard model including n.n hopping t and n.n.n hopping t'. This model was solved using DMFT with CTQMC , and the mean-field slave boson approach. Even a small value of t'/t gives a significant impact on the stability of Nagaoka ferromagnetism. The DMFT result shows that the ferromagnetic state becomes more stable for negative t'/t, and this is supported by a slave boson solution (see Table 1) and can also be understood from a diagonalization of a 4-site plaquette. The energy of the minimum spin state ($S=1/2$) depends weakly on t'/t, while the energy of the maximum spin state ($S=3/2$) depends linearly on t'/t. Therefore, the maximum spin state becomes more stable for negative t'/t.

In both slave boson and DMFT methods, paramagnetic energy does not vary much as t'/t changes due to the strong renormalization of the quasiparticle band (see Fig. 10). However, fully polarized ferromagnetic energy depends on t'/t because the spectral function becomes

similar to the non-interacting one in a fully polarized spin state. At $t'/t < 0$, the high spectral peak of the non-interacting DOS in the low energy region makes the FM energy more stable than a $t'/t \geq 0$ case.

Within DMFT, the nature of the transition also varies with t'/t. A first order transition accompanying the PS of the FM and PM state occurs when $t'/t = -0.1$ while a second order transition occurs when $t'/t = 0$. In the slave boson approach, the transition is always first order regardless of t'/t. This is because the slave boson method overestimates the PM energy. The DMFT result shows that when $n \to 1$, the FM state becomes unstable as T exceeds T_{coh}. In other words, ferromagnetic state is only stable within the coherent Fermi liquid regime.

The $U = \infty$ one band Hubbard model is a toy model and does not describe any specific material. However it is physically realizable in an optical lattice, due to the recent developments in controlling cold atoms in optical traps[26,27]. These systems are highly tunable, and the hopping parameter t and the on-site interaction U can be adjusted by varying the ratio of the potential depth of the optical lattice to the recoil energy (V_0/E_R) or the ratio of interatomic scattering length to the lattice spacing (a_s/d). In order to realize the one-band Hubbard model with a large U ($U/t \geq 100$), $V_0/E_R \approx 30$ and $a_s/d \leq 0.01$ should be the range of parameters in the optical lattice (See Fig. 4 of Ref. 27). The tuning of the next-nearest neighbor hopping t' can be achieved by engineering optical lattices with a non-separable laser potential over each coordinate axis.

It will be very interesting to test these DMFT results experimentally. Usually, the atomic trap potential is applied to confine atoms in the optical lattice, and the potential varies smoothly having the minimum at the center of the trap. The phase separation between the FM and the PM phase at $t'/t = -0.1$ (taking place between the densities $n = 0.696 - 0.715$) can be observed in the optical lattice as three spatially separated distinct regions. The atom-rich FM region will tend to move to the center of the optical lattice to be energetically stabilized while the hole-rich PM region will reside on the edge of the optical lattice. Since the total spin is a conserved quantity, the FM region which will be located at the center of the trap, and will consist of two domains containing the up or down species. Raising the temperature will destroy the ferromagnetic magnetic state and consequently the spatial patterns within the trap.

ACKNOWLEDGMENT

[1] Y. Nagaoka, Phys. Rev. **147**, 392 (1966).

[2] For recent reviews see : P. Fazekas, *Lecture Notes on Electron Correlation and Magnetism*, Series in Modern Condensed Matter Physics - Vol. 5 (World Scientific, 1999)

[3] B.S. Shastry, H.R. Krishnamurthy, and P.W. Anderson, Phys. Rev. B **41**, 2375 (1990).

[4] A.G. Basile and V. Elser, Phys. Rev. B **41**, 4842 (1990).

[5] W. von der Linden and D. Edwards, J. Phys. Condens. Matter. **3**, 4917 (1991).

[6] T. Hanisch and E. Muller-Hartmann, Ann. Phys **2**, 381 (1993).

[7] P. Wurth, G. Uhrig, and E. Mueller-Hartmann, Ann. Phys. **5**, 148 (1996).

[8] B. Moller, K. Doll, and R. Fresard, J. Phys., Condens. Matter. **5**, 4847 (1993).

[9] D. Boies, F. Jackson, and A.-M. Tremblay, Int. J. Mod. Phys. B **9**, 1001 (1995).

[10] X.Y. Zhang, E. Abrahams, and G. Kotliar, Phys. Rev. Lett. **66**, 1236 (1991).

[11] F. Becca and S. Sorella, Phys. Rev. Lett. **86**, 3396 (2001).

[12] A.M. Oles and P. Prelovsek, Phys. Rev. B **43**, 13348 (1991).

[13] H. Tasaki, Phys. Rev. Lett. **69**, 1608 (1992).

[14] T. Hanisch, G.S. Uhrig, and E. Muller-Hartmann, Phys. Rev. B **56**, 13960 (1997).

[15] J. Wahle, N. Blumer, J. Schlipf, K. Held, and D. Vollhardt, Phys. Rev. B **58**, 12749 (1998).

[16] L. Arrachea, Phys. Rev. B **62**, 10033 (2000).

[17] M. Ulmke, Eur. Phys. J. B **1**, 301 (1998).

[18] T. Wegner, M. Potthoff, and W. Nolting, Phys. Rev. B **57**, 6211 (1998).

[19] R. Hlubina, S. Sorella, and F. Guinea, Phys. Rev. Lett. **78**, 1343 (1997).

[20] T. Obermeier, T. Pruschke, and J. Keller, Phys. Rev. B **56**, R8479 (1997).

[21] R. Zitzler, T. Pruschke, and R. Bulla, Eur. Phys. J. B **27**, 473 (2002).

[22] P. Werner, A. Comanac, L. de'Medici, M. Troyer, and A.J. Millis, Phys. Rev. Lett. **97**, 076405 (2006).

[23] K. Haule, Phys. Rev. B **75**, 155113 (2007).

[24] M. Jarrell and J. Gubernatis, Phys. Rep. **269**, 133 (1996).

[25] H. Kajueter, G. Kotliar, and G. Moeller, Phys. Rev. B **53**, 16214 (1996).

[26] D. Jaksch and P. Zoller, Ann. Phys. **315**, 52 (2005).

[27] A. Georges, cond-mat/0702122 (2007).